

# Deformation behavior of friction-stir welded Al-Mg-Mn alloy with ultrafine-grained structure

I. Vysotskii, S. Malopheyev<sup>\*</sup>, S. Mironov, R. Kaibyshev

Belgorod National Research University, Pobeda 85, Belgorod 308015, Russia

## ARTICLE INFO

### Keywords:

Aluminum alloy  
Equal-channel angular pressing (ECAP)  
Ultrafine-grained structure  
Friction stir welding (FSW)  
Mechanical properties

## ABSTRACT

Low-temperature friction-stir welding (FSW) was successfully applied for the joining of Al-Mg-Mn alloy with an ultrafine-grained microstructure. The low-temperature conditions preserved fine-grained microstructure and nano-scale second-phase particles in the stir zone and thus provided nearly-100% joint efficiency of the produced welds. The deformation behavior of the welded joints was studied via the digital image correlation technique. The strengthening mechanisms of the base material and the stir zone material were examined.

## 1. Introduction

Due to the attractive combination of excellent mechanical characteristics at ambient conditions and superplastic properties at elevated temperatures, bulk ultrafine-grained (UFG) aluminum alloys are sometimes considered the next-generation materials [1,2]. However, the relatively small size of the material pieces that could be produced by the available processing techniques, significantly restricts their commercial applications. In this context, a joining of several UFG sheets into a single package may be a possible solution to this problem.

Friction-stir welding (FSW) e.g. [3–6] is often considered the most prominent candidate for this purpose. This approach avoids material melting but, in contrast, involves very large plastic strains and therefore may retain the UFG structure nearly unchanged. Indeed, the first results in this area were in good accordance with expectations, i.e., FSW typically led to only subtle microstructural coarsening in the stir zone [7–17]. Nevertheless, an essential material softening was typically observed [7–17], presumably due to the dynamic recrystallization occurring during the welding process. It may be suggested, therefore, that only low-heat-input FSW is suitable for successful joining of the UFG materials. To date, only limited works have been reported in this field, which typically confirm the enhanced mechanical properties of the low-temperature FSW joints [11,16]. It should be noted, however, that the underlying mechanism of the microstructural evolution during low-

temperature welding of UFG materials is still not clear, and therefore, this issue obviously warrants further study.

It is worth noting that the second-phase particles are well-known to suppress the recrystallization processes in friction-stir welded materials via grain-boundary pinning e.g., [18–20]. Hence, the low-heat-input FSW seems to be particularly effective for the particle-containing UFG alloys. Although the above conception is remarkably simple, its feasibility has not been proven experimentally so far. Therefore, the purpose of the present study was to examine the efficiency of the low-temperature FSW for joining of a typical UFG material that contained fine unsolvable dispersoids.

## 2. Material and experimental procedures

The Zr-modified commercial AA5083 alloy with a measured chemical composition of Al-5.4%Mg-0.5%Mn-0.1%Zr-0.12%Si-0.014%Fe (all in wt%) was produced by direct chill casting. To obtain the UFG structure, the cast ingot was homogenized at 360 °C for 6 h [21,22] and then subjected to equal-channel angular pressing (ECAP) at 300 °C to the true strain of ~12 using the B<sub>C</sub> route [21]. The 2-mm-thick sheets of the ECAPed material were butt-welded parallel to the pressing direction employing a commercial AccuStir 1004 FSW machine. The welding tool consisted of a shoulder with a diameter of 12.5 mm and an M5 cylindrical probe of 1.7 mm in length. To keep the welding temperature as

<sup>\*</sup> Corresponding author.

E-mail address: [malofeev@bsu.edu.ru](mailto:malofeev@bsu.edu.ru) (S. Malopheyev).

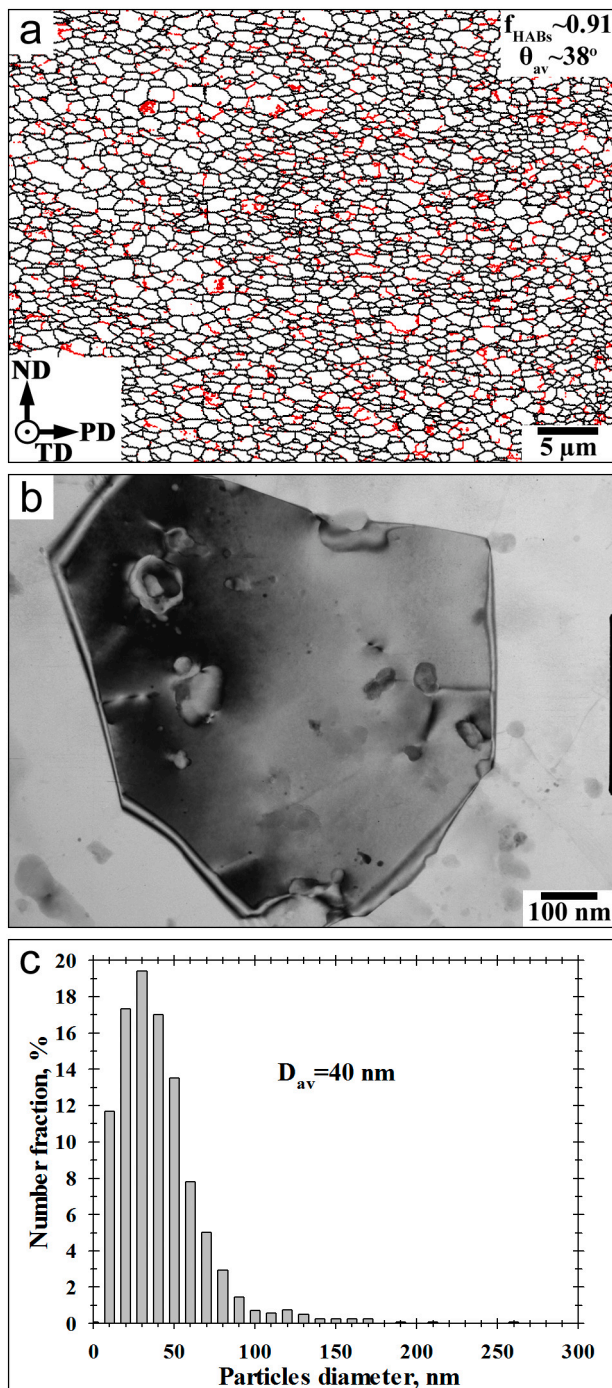


Fig. 1. Microstructure of the base material: (a) EBSD grain-boundary map, (b) TEM micrograph, and (c) the particle-size distribution.

low as possible but avoid welding defects, FSW was conducted at a tool rotation rate of 500 rpm and a tool travel speed of 125 mm/min. These particular welding variables were selected on the basis of the previous experiments.<sup>1</sup> Though welding temperature was not measured in the present study, from the authors' previous experience of working with various aluminum alloys e.g. [23], it unlikely exceeded 400 °C.

Microstructural examinations were performed by optical microscopy, electron backscatter diffraction (EBSD), and transmission electron microscopy (TEM). The metallographic observations were carried out using an Olympus GX71 optical microscope. High-resolution EBSD analysis was conducted using an FEI Quanta 600 field-emission-gun scanning electron microscope (FEG-SEM) equipped with TSL OIM™ software. The TEM study was performed using a JEM-2100EX TEM operating at 200 kV. The suitable surface for the EBSD and TEM observations was obtained by mechanical polishing in a conventional fashion followed by electro-polishing using a 25% nitric-acid solution in ethanol at −32 °C (241 K) and a voltage of 19.5 V. In the EBSD maps shown in this paper, low-angle boundaries (LABs) ( $2^\circ < \theta < 15^\circ$ ) and high-angle boundaries (HABs) ( $\theta \geq 15^\circ$ ) were depicted as red and black lines, respectively. Dislocation density was measured by TEM using the point count technique [24].

To view microstructure distribution in the weld zone more broadly, microhardness profiles were measured across the weld transverse cross-section at the mid-thickness of the welded joints. Vickers microhardness data was obtained by applying a load of 100 g with a dwell time of 15 s in a Wolpert 402MVD microhardness tester.

The mechanical properties and deformation behavior of the produced joint were examined using transverse tensile tests according to the ASTM E8M standard. To this end, tensile specimens were machined perpendicular to the welding direction (WD), and the gauge section of the specimens included all characteristic FSW zones. To examine the mechanical properties of the stir zone material, the specimens were machined along with the WD and included the stir-zone material only. In all cases, the specimens had a gauge section of 35 mm in length and  $5 \times 2 \text{ mm}^2$  in cross-section. The face surfaces of all tensile specimens were mechanically polished to achieve a uniform thickness and eliminate surface defects. Tension tests to failure were conducted at ambient conditions using an Instron 5882 universal testing machine equipped with an automatic extensometer MFX500. Three tensile specimens were tested for each material condition.

In order to investigate the distribution of local strains produced during the tensile tests, the digital image correlation (DIC) technique was employed. To this end, a random ink pattern was applied to the specimens' surfaces, and two high-speed digital cameras were used for recording the changes occurring in such patterns during the tensile tests. The in-plane Lagrangian strains were measured using a commercial Vic-3D™ system by Correlated Solutions, Inc.

Further experimental details are available in the previous works [7,21,22].

### 3. Results

#### 3.1. Base material

The UFG microstructure produced during ECAP is shown in Fig. 1. The microstructure consisted of low-aspect-ratio grains with a mean size

<sup>1</sup> It is often believed that the peak FSW temperature is mainly governed by the tool rotation rate, whereas the cooling speed is primarily controlled by the welding speed. Hence, to provide the low-heat-input condition, it is necessary to keep the spindle rate as low as possible, whereas the feed rate should be the highest. On the other hand, the excessive lowering of the FSW temperature typically leads to volumetric defects. On the basis of extensive preliminary experiments, it was found that the optical welding conditions include a tool rotation rate of 500 rpm and a tool travel speed of 125 mm/min.

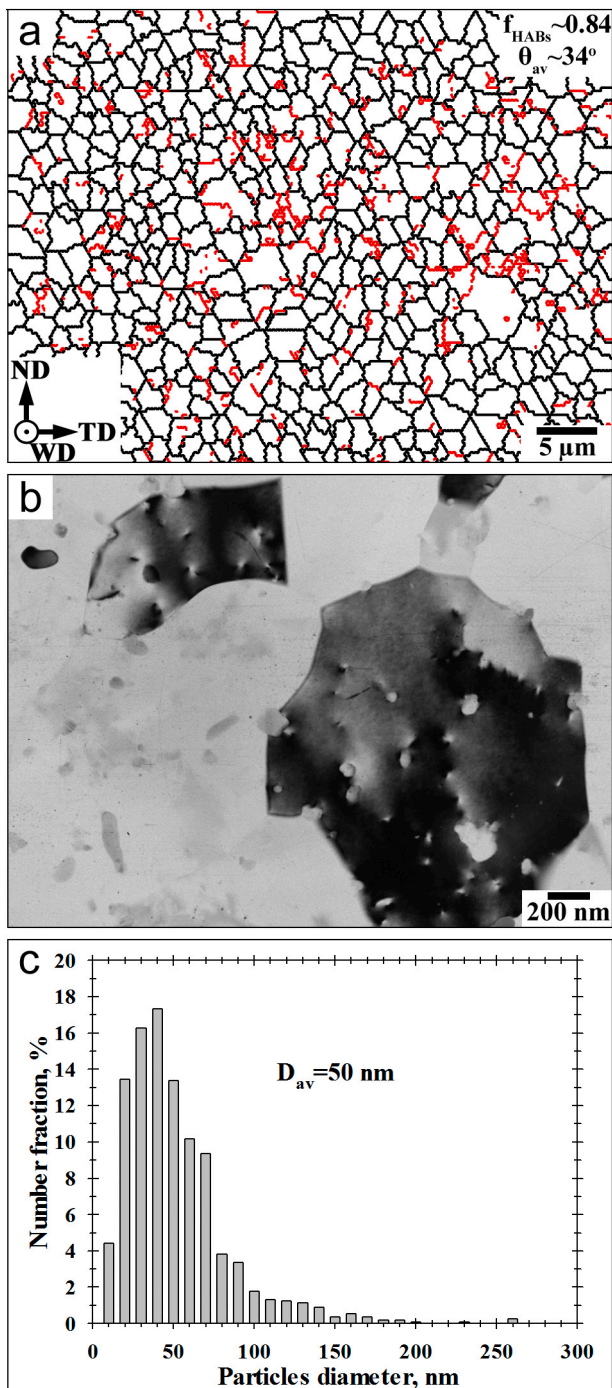


Fig. 2. Microstructure of the stir-zone material: (a) EBSD grain-boundary map, (b) TEM micrograph, and (c) the particle-size distribution.

of  $\sim 1.1 \mu\text{m}$ , which contained only a poorly developed substructure (Fig. 1a). Specifically, the LAB fraction was measured to be  $\sim 9\%$ , whereas the dislocation density was as low as  $\sim 4 \times 10^{13} \text{m}^{-2}$ . TEM observation revealed the incoherent  $\text{Al}_6\text{Mn}$  dispersoids of  $\sim 40 \text{nm}$  in average diameter and of  $\sim 0.09\%$  in volume fraction, which were evenly distributed in the grain interiors (Fig. 1b and c). Previous research [21,22] has demonstrated that these nano-scale particles play a crucial role in microstructural refinement during ECAP. The prior homogenization of the cast ingot at a relatively low temperature of  $360 \text{ }^\circ\text{C}$  (as indicated in Section 2) prevented the constituent  $\text{Al}_6\text{Mn}$  precipitates from excessive coarsening. Hence, due to the relatively high Zener force, the particles efficiently pinned grain boundaries during ECAP and thus

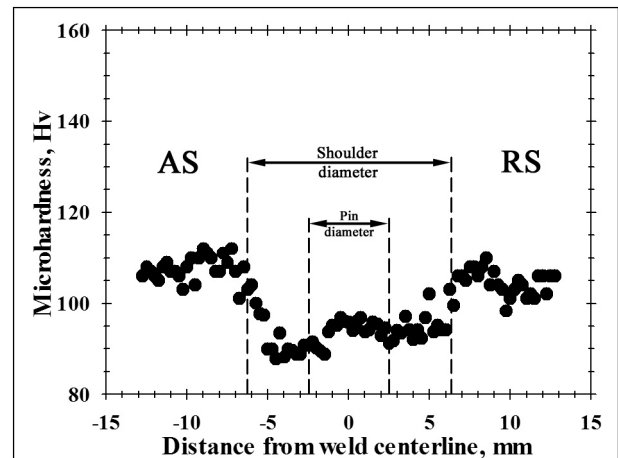


Fig. 3. Microhardness profile measured across the joint mid-thickness. AS and RS denote the advancing- and retreating sides, respectively.

promoted the formation of the fine-grained structure.

### 3.2. Stir zone

The microstructure produced in the stir zone after FSW was dominated by the almost fully recrystallized equiaxed grains of  $\sim 1.8 \mu\text{m}$  in diameter (Fig. 2a). As compared to the base material state, the LAB fraction somewhat increased up to  $\sim 16\%$ , whereas the dislocation density was reduced to  $\sim 1 \times 10^{13} \text{m}^{-2}$ . The reason for the disclosed increase in the LAB content is not clear. One of the possible explanations may be the relatively high temperature of the FSW process. As shown recently [25], this may promote the activation of recovery mechanisms that reduce dislocation density and thus retard the transformation of LABs into HABs.

Importantly, the nanoscale  $\text{Al}_6\text{Mn}$  particles were retained nearly unchanged (Fig. 2b) showing only a subtle increase in the mean diameter up to  $50 \text{nm}$  (Fig. 2c). This effect was apparently due to the relatively low welding temperature employed in the present study, which prevented the dispersoids from excessive coarsening.<sup>2</sup> Of particular interest was the observation that the precipitates were often distributed along grain boundaries (Fig. 2b) thus presumably pinning grain growth in the stir zone.

Thus, it is evident that the fine-grained structure was essentially preserved during FSW. In addition to the relatively low-temperature character of the welding process, this effect is thought to also be contributed by the pinning effect of the  $\text{Al}_6\text{Mn}$  dispersoids.

### 3.3. Microhardness profile

Fig. 3 shows the microhardness profile measured across the weld mid-thickness. For clarity reasons, the shoulder diameter and probe diameter were also indicated in the figure. To the first approximation, the probe diameter outlines the stir zone, whereas the shoulder diameter delineates the heat-affected zone.

Despite the low-heat-input welding condition employed in the present study, it is seen that FSW provided notable material softening. Specifically, the average microhardness decreased from  $\sim 105 \text{Hv}$  in the base material to  $\sim 95 \text{Hv}$  in the stir zone. Remarkably, the softened region encompassed not only the stir zone but also included the heat-affected zone. It is also worth noting that the softening effect was most pronounced on the advancing side of the weld.

<sup>2</sup> According to ThermoClac calculations (supplementary Fig. S1), the volume fraction of  $\text{Al}_6\text{Mn}$  particles should experience only a minor change during FSW.

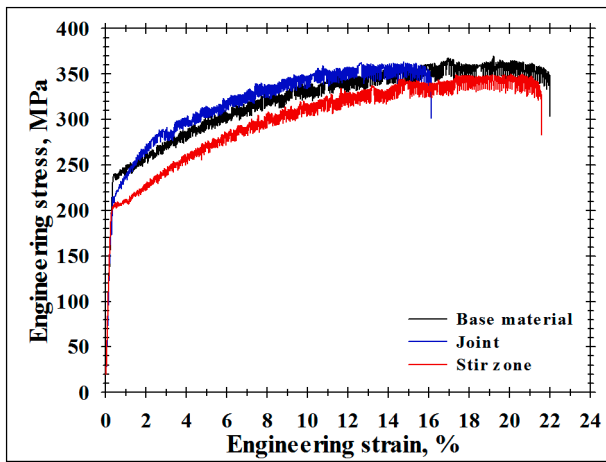


Fig. 4. Typical tensile diagrams for the UFG base material, FSW joint, and the stir zone material.

**Table 1**  
Mechanical properties of the base material, FSW joint and the stir zone material.

Material condition	Yield strength, MPa	Ultimate tensile strength, MPa	Ductility, %	Joint efficiency, %	
				For yield strength	For ultimate tensile strength
Base material	235 ± 1	370 ± 2	21 ± 2	–	–
FSW joint	220 ± 1	365 ± 2	15.7 ± 2	94	99
Stir zone	205 ± 1	350 ± 2	21 ± 2	–	–

Note. Error shows instrumental accuracy of measurements.

3.4. Tensile test

Typical tensile diagrams of the base material, the welded joint, and the stir-zone material are shown in Fig. 4. The relevant mechanical properties are summarized in Table 1. In all studied conditions, the material exhibited the jerky flow phenomenon (Fig. 4), which is usually attributed to the Portevin-Le Chatelier (PLC) effect [26]. The magnitude

of the stress oscillations increased with tensile strain, i.e., the serrations resembled the type B behavior of the PLC effect. In the case of the welded joint, the deformation diagram was characterized by relatively high strain hardening at small tensile strains, but then it changed to the rate close to the base material (Fig. 4). On the other hand, the base material and the stir-zone material exhibited relatively monotonic strain hardening behavior in comparison with the presence of a kink in the case of the welded joint (Fig. 4).

Remarkably, the base material and the stir zone material exhibited broadly similar ductility (Fig. 4). This effect is thought to additionally reflect a close resemblance of the microstructures in both material conditions (Figs. 1 and 2).

Of particular importance was the observation that the joint efficiency for the FSW joint was measured to be 94% for the yield strength and even 99% for the ultimate tensile strength (Table 1), thus being relatively high. It is also worth noting that the reduction in the yield strength (i.e., ~6%) was comparable with the decrease in microhardness (i.e., ~10%, Fig. 3).

3.5. Digital-image correlation measurements

To provide additional insight into the tensile behavior of the welded material, the digital image correlation technique was applied. The typical results are shown in Fig. 5.

It is seen that the material flow during the tensile tests was characterized by an inhomogeneous strain distribution. Specifically, the strain was initiated at the advancing side of the weld (Fig. 5a), which was the softest microstructural region according to the microhardness measurements (Fig. 3).

With the increase in the global tensile elongation, the plastic strain rapidly encompassed the entire weld zone (Fig. 5b) and then propagated to the base material region (Fig. 5c). This effect was clearly related to both (a) the relatively small difference in strength between the stir zone and the base material (10%, as discussed in Section 3.3) and (b) the comparatively high strain hardening observed at the early stage of tensile deformation of the FSW joint (Fig. 4). It is important to emphasize that Fig. 5c corresponded to the kink on the deformation curve where the work hardening became similar to that for the base materials. Considering the relatively low strain hardening capacity of the stir zone material per se (Fig. 4), the origin of the revealed strain propagation is not completely clear.

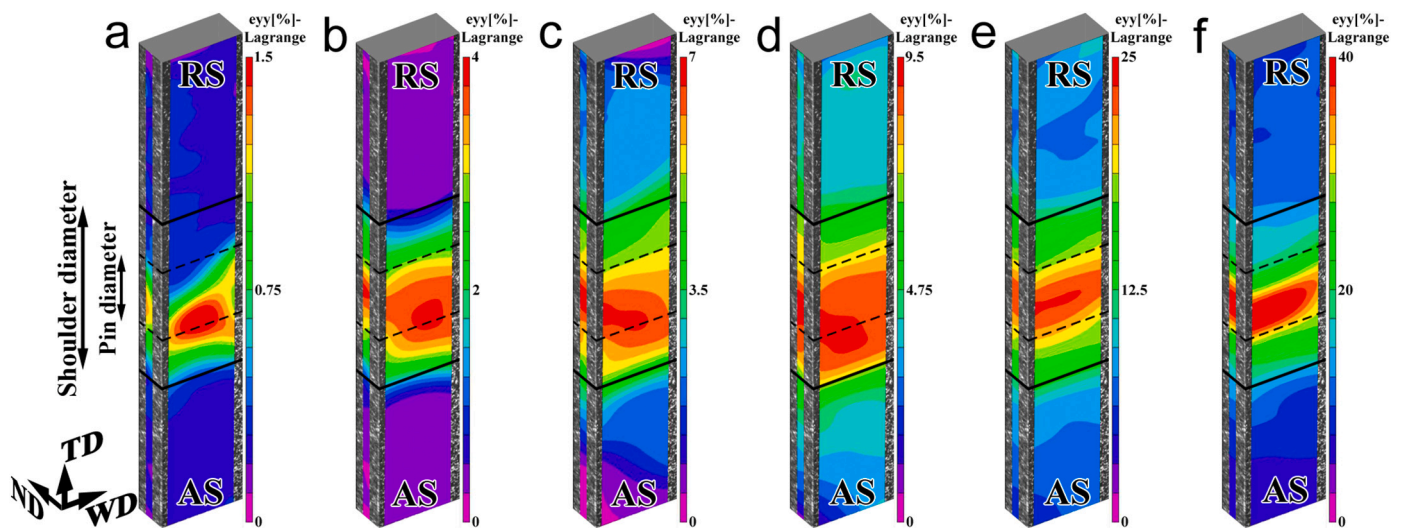


Fig. 5. Typical distribution of local longitudinal strains on the shoulder side and the cross-section side of the FSW joint, which evolved during transverse tensile tests after global elongation of 0.2% (a), 1% (b), 3% (c), 5% (d), 11% (e), and immediately before failure (f). WD, TD and ND refer to welding direction, transverse direction, and normal direction, respectively. AS and RS denote advancing and retreating sides, respectively. For simplicity, probe diameter and shoulder diameter are indicated. Note: Tensile direction is vertical.

**Table 2**  
Contribution of strengthening mechanisms in the base material and the stir zone material.

Material condition	Calculated strengthening, MPa					Experimental yield stress, MPa
	Solid-solution	Precipitation	Dislocation	Grain-boundary	Total	
Base material	98.5	11.5	38	110	268	235
Stir zone	98.5	9.5	17	82	217	205

As follows from the works by Sato et al. [27] and Kar et al. [28], the tensile properties of friction-stir welds are usually governed by the softest microstructural region. This concept has been confirmed in numerous studies, thus being beyond any doubt. Hence, the effect revealed in the present study was somewhat unusual. On the other hand, it was observed in all three tested specimens, so the authors are hopeful that this phenomenon is real. One of the possible explanations for it may be the back stresses that were presumably generated between the differently-strained stir zone and the base material zone during the tensile test. It is thought that the plastic deformation of heterogeneous structures can cause significant internal (i.e., back-) stresses, which can significantly affect deformation behavior e.g., [29]. On the other hand, this assumption in the context of the present work is entirely speculative, and therefore, the revealed effect obviously warrants further study.

Anyway, the propagation of the tensile strain into the base material region provided excellent joint efficiency in terms of the ultimate tensile strength (~99%) revealed during the tensile tests (Table 1).

Despite the propagation of the plastic strain across the entire tensile specimen, the strain was still most pronounced at the advancing side of the weld (Fig. 5d and e), which caused the final failure in this microstructural region (Fig. 5f). This observation was probably attributable to the relatively low strain-hardening rate of the stir zone material, as mentioned above.

#### 4. Discussion

In order to get a quantitative insight into the strength of the welded material, the mutual contributions of different strengthening mechanisms were evaluated. Assuming that these mechanisms act independently, the yield strength of the examined material may be represented as follows [22,30]:

$$\sigma_{0.2} = \sigma_0^{Al} + \sigma_{SS} + \sigma_p + \sigma_d + \sigma_{GB} \quad (1)$$

where  $\sigma_0^{Al}$  is the lattice friction stress of high-purity aluminum (~10 MPa [31,32]),  $\sigma_{SS}$  is solid solution strengthening,  $\sigma_p$  is precipitation hardening,  $\sigma_d$  is dislocation strengthening, and  $\sigma_{GB}$  is grain-boundary strengthening.

The solid solution strengthening in aluminum alloys is often believed to be mainly contributed by magnesium and manganese solutes and could be expressed as follows [22,33]:

$$\sigma_{SS} = \sigma_{trace} + H_{Mg} C_{Mg}^n + H_{Mn} C_{Mn}^m \quad (2)$$

where  $\sigma_{trace}$  is the strengthening effects of trace elements (~24 MPa [31]),  $H_{Mg}$  is the hardening efficiency of magnesium (~13.8 MPa/(wt% Mg) [32]),  $C_{Mg}$  is concentration of Mg in weight percent,  $n$  is the strengthening exponent (~1 for Al-Mg alloys [34,35]),  $H_{Mn}$  is the hardening efficiency of manganese (~18.35 MPa/(wt% Mn) [32]),  $C_{Mn}$  is the concentration of Mn in weight percent, and  $m$  is another strengthening exponent (~0.9 for the Al-Mg alloys [33,35]).

In the Al-Mg-Mn alloys (including the examined material), the precipitation strengthening is mainly associated with incoherent Al<sub>6</sub>Mn particles [36] and could be quantified in terms of the Orowan bowing mechanism [34]:

$$\sigma_p = \frac{0.4Mgb}{\pi\lambda} \frac{\ln(2\bar{r}/b)}{\sqrt{1-\nu}} \quad (3)$$

where  $M$  is the Taylor factor (~3.06),  $G$  is shear modulus of aluminum (~25.4 GPa),  $b$  is the Burgers vector (~0.286 nm),  $\lambda$  is the mean particle spacing,  $\bar{r} = \sqrt{2/3}r$  is the mean radius of a circular cross section in a random plane for a spherical precipitate,  $r$  is the average particle diameter, and  $\nu$  is Poisson's ratio for aluminum (=0.33).

Assuming a random distribution of the dispersoids, the mean edge-to-edge inter-particle distance could be estimated as [34].

$$\lambda = 2\bar{r} \left( \sqrt{\frac{\pi}{2f}} - 1 \right), \quad (4)$$

where  $f$  is the particle volume fraction. From the calculations, it was found that  $\lambda$  in the base material was ~1.41 μm whereas that in the stir zone was ~1.77 μm. These results were comparable with that reported by Sato et al. [13].

The dislocation strengthening is usually described in terms of the Taylor law [22,31,34,36]:

$$\sigma_d = \alpha M G b \rho^{1/2} \quad (5)$$

where  $\alpha$  is a constant (~0.24), and  $\rho$  is density of free dislocations.

The contribution of the grain boundary strengthening is usually expressed in terms of the Hall-Petch relationship [1,6,13,22,32,36]:

$$\sigma_{GB} = k_y d_{GB}^{-1/2} \quad (6)$$

where  $k_y$  is the Hall-Petch slope (taken to be ~0.11 MPa × m<sup>1/2</sup> [22]), and  $d_{GB}$  is the average HAB spacing.

The calculated contributions of the strengthening mechanisms and the measured yield strengths of both the base material and the stir zone materials were summarized in Table 2. The acceptable agreement between the predictions and the experimental results is worthy of the remark. From the calculations, it is seen that the relatively high strength of the stir zone material was mainly associated with the preservation of the fine-grained microstructure. On the other hand, the contribution of the precipitation hardening was relatively small. Hence, it is likely that the principal role of Al<sub>6</sub>Mn particles was the suppression of the microstructural coarsening in the stir zone thus indirectly contributing to the grain-boundary strengthening. It is also worth noting that the crucial role played by the Al<sub>6</sub>Mn particles in the Hall-Petch relationship for the friction-stir welded 5xxx aluminum alloys has been first emphasized by Sato et al. [13,37].

As shown in Section 3.3, the material softening within the weld zone was most pronounced on the advancing side of the heat-affected zone (Fig. 3). In the context of the above considerations, it is likely that this effect was associated with either prominent grain coarsening and/or static recrystallization in this microstructural region. This assumption is in line with typical temperature measurements and numerical simulations, which show an increased welding temperature in this area. In the present work, however, this idea has not been proven experimentally, and therefore this issue requires further investigation.

#### 5. Conclusion

In this work, low-temperature FSW was applied to preserve the unique mechanical characteristics of a UFG aluminum alloy during welding. The main conclusions derived from this work are as follows:

- (1) Despite the marginal microstructural coarsening that was observed in the welded material due to the FSW heat input, the fine-grained microstructure and the constituent nano-scale particles were preserved.
- (2) The joint efficiency of the produced weld was found to be as high as 99%. The low-heat-input FSW is highly feasible for the joining of UFG materials.

### Declaration of Competing Interest

The authors declare that they have no known competing financial interests or personal relationships that could have appeared to influence the work reported in this paper.

### Acknowledgements

The study was supported by a grant from the Russian Science Foundation No. 21-79-10088 (<https://rscf.ru/en/project/21-79-10088/>). The authors are grateful to the staff of the Joint Research Center (JRC) "Technology and Materials" at Belgorod State National Research University for their assistance with the structural and mechanical characterizations.

### Appendix A. Supplementary data

Supplementary data to this article can be found online at <https://doi.org/10.1016/j.matchar.2022.111758>.

### References

- [1] R.Z. Valiev, A.P. Zhilyaev, T.G. Langdon, *Bulk Nanostructured Materials: Fundamentals and Applications*, TMS-Wiley, Hoboken, New Jersey, 2014.
- [2] M. Kawasaki, T.G. Langdon, Review: achieving superplastic properties in ultrafine-grained materials at high temperatures, *J. Mater. Sci.* 51 (2016) 19–32, <https://doi.org/10.1007/s10853-015-9176-9>.
- [3] R.S. Mishra, Z.Y. Ma, Friction stir welding and processing, *Mater. Sci. Eng. R* 50 (2005) 1–78, <https://doi.org/10.1016/j.mser.2005.07.001>.
- [4] A. Heidarzadeh, S. Mironov, R. Kaibyshev, G. Çam, A. Simar, A. Gerlich, F. Khodabakhshi, A. Mostafaei, D.P. Field, J.D. Robson, A. Deschamps, P. J. Withers, Friction stir welding/processing of metals and alloys: A comprehensive review on microstructural evolution, *Prog. Mater. Sci.* 117 (2021), 100752, <https://doi.org/10.1016/j.pmatsci.2020.100752>.
- [5] Y. Chen, H. Wang, X. Wang, H. Ding, J. Zhao, F. Zhang, Z. Ren, Influence of tool pin eccentricity on microstructural evolution and mechanical properties of friction stir processed Al-5052 alloy, *Mater. Sci. Eng. A* 739 (2019) 272–276, <https://doi.org/10.1016/j.msea.2018.10.057>.
- [6] Y. Chen, H. Ding, J. Li, Z. Cai, J. Zhao, W. Yang, Influence of multi-pass friction stir processing on the microstructure and mechanical properties of Al-5083 alloy, *Mater. Sci. Eng. A* 650 (2016) 281–289, <https://doi.org/10.1016/j.msea.2015.10.057>.
- [7] S. Malopheyev, S. Mironov, V. Kulitskiy, R. Kaibyshev, Friction-stir welding of ultra-fine grained sheets of Al–Mg–Sc–Zr alloy, *Mater. Sci. Eng. A* 624 (2015) 132–139, <https://doi.org/10.1016/j.msea.2014.11.079>.
- [8] S. Malopheyev, S. Mironov, I. Vysotskiy, R. Kaibyshev, Superplasticity of friction-stir welded Al–Mg–Sc sheets with ultrafine-grained microstructure, *Mater. Sci. Eng. A* 649 (2016) 85–92, <https://doi.org/10.1016/j.msea.2015.09.106>.
- [9] Y.S. Sato, Y. Kurihara, S.H.C. Park, H. Kokawa, N. Tsuji, Friction stir welding of ultrafine grained Al alloy 1100 produced by accumulative roll-bonding, *Scr. Mater.* 50 (2004) 57–60, <https://doi.org/10.1016/j.scriptamat.2003.09.037>.
- [10] M. Lipińska, L. Olejnik, A. Pietras, A. Rosochowski, P. Bazarnik, J. Goliński, T. Brynk, M. Lewandowska, Microstructure and mechanical properties of friction stir welded joints made from ultrafine grained aluminium 1050, *Mater. Des.* 88 (2015) 22–31, <https://doi.org/10.1016/j.matdes.2015.08.129>.
- [11] C.Y. Liu, B. Qu, P. Xue, Z.Y. Ma, K. Luo, M.Z. Ma, R.P. Liu, Fabrication of large-bulk ultrafine grained 6061 aluminum alloy by rolling and low-heat-input friction stir welding, *J. Mater. Sci. Technol.* 34 (2018) 112–118, <https://doi.org/10.1016/j.jmst.2017.02.008>.
- [12] I. Topic, H.W. Höppel, M. Göken, Friction stir welding of accumulative roll-bonded commercial-purity aluminium AA1050 and aluminium alloy AA6016, *Mater. Sci. Eng. A* 503 (2009) 163–166, <https://doi.org/10.1016/j.msea.2007.12.057>.
- [13] Y.S. Sato, M. Urata, H. Kokawa, K. Ikeda, Hall–Petch relationship in friction stir welds of equal channel angular-pressed aluminium alloys, *Mater. Sci. Eng. A* 354 (2003) 298–305, [https://doi.org/10.1016/S0921-5093\(03\)00008-X](https://doi.org/10.1016/S0921-5093(03)00008-X).
- [14] R. Uejii, H. Fujii, L. Cui, A. Nishioka, K. Kunishige, K. Nogi, Friction stir welding of ultrafine grained plain low-carbon steel formed by the martensite process, *Mater. Sci. Eng. A* 423 (2006) 324–330, <https://doi.org/10.1016/j.msea.2006.02.038>.
- [15] H. Fujii, R. Uejii, Y. Takada, H. Kitahara, N. Tsuji, K. Nakata, K. Nogi, Friction stir welding of ultrafine grained interstitial free steels, *Mater. Trans.* 47 (2006) 239–242, <https://doi.org/10.2320/matertrans.47.239>.
- [16] M. Hosseini, H. Danesh Manesh, Immersed friction stir welding of ultrafine grained accumulative roll-bonded Al alloy, *Mater. Design* 31 (2010) 4786–4791, <https://doi.org/10.1016/j.matdes.2010.05.007>.
- [17] S. Sabooni, F. Karimzadeh, M.H. Enayati, A.H.W. Ngan, Friction-stir welding of ultrafine grained austenitic 304L stainless steel produced by martensitic thermomechanical processing, *Mater. Design* 76 (2015) 130–140, <https://doi.org/10.1016/j.matdes.2015.03.052>.
- [18] A. Kar, S.V. Kailas, S. Suwas, Mechanism of variation in high-temperature grain stability of aluminum in dissimilar friction stir welds, *Mater. Perform. Character.* 6 (2020) 20190011, <https://doi.org/10.1520/MPC20190011>.
- [19] A. Kar, S. Suwas, S.V. Kailas, Microstructural Modification and High-Temperature Grain Stability of Aluminum in an Aluminum-Titanium Friction Stir Weld with Zinc Interlayer, *JOM*. 71 (2019) 444–451, <https://doi.org/10.1007/s11837-018-3152-1>.
- [20] A. Kar, D. Yadav, S. Suwas, S.V. Kailas, Role of plastic deformation mechanisms during the microstructural evolution and intermetallics formation in dissimilar friction stir weld, *Mater. Character.* 164 (2020), 110371, <https://doi.org/10.1016/j.matchar.2020.110371>.
- [21] I. Nikulin, A. Kipelova, S. Malopheyev, R. Kaibyshev, Effect of second phase particles on grain refinement during equal-channel angular pressing of an Al–Mg–Mn alloy, *Acta Mater.* 60 (2012) 487–497, <https://doi.org/10.1016/j.actamat.2011.10.023>.
- [22] S. Malopheyev, V. Kulitskiy, R. Kaibyshev, Deformation structures and strengthening mechanisms in an Al–Mg–Sc–Zr alloy, *J. Alloys Compd.* 698 (2017) 957–966, <https://doi.org/10.1016/j.jallcom.2016.12.289>.
- [23] A. Kalinenko, I. Vysotskiy, S. Malopheyev, S. Mironov, R. Kaibyshev, Influence of the weld thermal cycle on the grain structure of friction-stir joined 6061 aluminum alloy, *Mater. Character.* 178 (2021), 111202, <https://doi.org/10.1016/j.matchar.2021.111202>.
- [24] P.B. Hirsch, A. Howie, R.B. Nicholson, D.W. Pashley, M.J. Whelan, *Electron Microscopy of Thin Crystals*, 2nd ed., Krieger, New York, 1977.
- [25] S. Mironov, K. Inagaki, Y.S. Sato, H. Kokawa, Effect of welding temperature on microstructure of friction-stir welded aluminum alloy 1050, *Metall. Mater. Trans. A* 46 (2015) 783–790, <https://doi.org/10.1007/s11661-014-2651-0>.
- [26] D. Yuzbekova, A. Mogucheva, D. Zhemchuzhnikova, T. Lebedkina, M. Lebyodkin, R. Kaibyshev, Effect of microstructure on continuous propagation of the Portevin–Le Chatelier deformation bands, *Int. J. Plast.* 96 (2017) 210–226, <https://doi.org/10.1016/j.ijplas.2017.05.004>.
- [27] Y.S. Sato, H. Kokawa, Distribution of tensile property and microstructure in friction stir weld of 6063 aluminum, *Metall. Mater. Trans. A* 32 (2001) 3023–3031, <https://doi.org/10.1007/s11661-001-0177-8>.
- [28] A. Kar, S.V. Kailas, S. Suwas, Two-pass friction stir welding of aluminum alloy to titanium alloy: A simultaneous improvement in mechanical properties, *Mater. Sci. Eng. A* 733 (2018) 199–210, <https://doi.org/10.1016/j.msea.2018.07.057>.
- [29] X. Wu, M. Yang, F. Yuan, G. Wu, Y. Wei, X. Huang, Y. Zhu, Heterogeneous lamella structure unites ultrafine-grain strength with coarse-grain ductility, *Proc. Natl. Acad. Sci. U. S. A.* 112 (2015) 14501–14505, <https://doi.org/10.1073/pnas.1517193112>.
- [30] A. Mohammadi, N.A. Enikeev, M.Yu. Murashkin, M. Arita, K. Edalati, Examination of inverse Hall–Petch relation in nanostructured aluminum alloys by ultra-severe plastic deformation of an Al–La–Ce alloy, *J. Mater. Sci. Technol.* (2021), S1005030221003340, <https://doi.org/10.1016/j.jmst.2021.01.096>.
- [31] Y. Li, B. Hu, B. Liu, A. Nie, Q. Gu, J. Wang, Q. Li, Insight into Si poisoning on grain refinement of Al–Si/Al–5Ti–B system, *Acta Mater.* 187 (2020) 51–65, <https://doi.org/10.1016/j.actamat.2020.01.039>.
- [32] N. Kamikawa, X. Huang, N. Tsuji, N. Hansen, Strengthening mechanisms in nanostructured high-purity aluminium deformed to high strain and annealed, *Acta Mater.* 57 (2009) 4198–4208, <https://doi.org/10.1016/j.actamat.2009.05.017>.
- [33] E.L. Huskins, B. Cao, K.T. Ramesh, Strengthening mechanisms in an Al–Mg alloy, *Mater. Sci. Eng. A* 527 (2010) 1292–1298, <https://doi.org/10.1016/j.msea.2009.11.056>.
- [34] T.J. Harrell, T.D. Topping, H. Wen, T. Hu, J.M. Schoenung, E.J. Lavernia, Microstructure and strengthening mechanisms in an ultrafine grained Al–Mg–Sc alloy produced by powder metallurgy, *Metall. Mater. Trans. A*. 45 (2014) 6329–6343, <https://doi.org/10.1007/s11661-014-2569-6>.
- [35] O. Ryen, B. Holmedal, O. Nijis, E. Nes, E. Sjölander, H.-E. Ekström, Strengthening mechanisms in solid solution aluminum alloys, *Metall. Mater. Trans. A*. 37 (2006) 1999–2006.
- [36] S. Malopheyev, R. Kaibyshev, Strengthening mechanisms in a Zr-modified 5083 alloy deformed to high strains, *Mater. Sci. Eng. A* 620 (2015) 246–252, <https://doi.org/10.1016/j.msea.2014.10.030>.
- [37] Y.S. Sato, S.H.C. Park, H. Kokawa, Microstructural factors governing hardness in friction-stir welds of solid-solution-hardened Al alloys, *Metall. Mater. Trans. A* 32 (2001) 3033–3042, <https://doi.org/10.1007/s11661-001-0178-7>.